Research Article

Mazin Aljazzazi, Banan Maayah, Nadir Djeddi, Mohammed Al-Smadi*, and Shaher Momani

A novel numerical approach to solutions of fractional Bagley-Torvik equation fitted with a fractional integral boundary condition

https://doi.org/10.1515/dema-2022-0237
received April 8, 2022; accepted April 28, 2023

Abstract: In this work, we present a sophisticated operating algorithm, the reproducing kernel Hilbert space method, to investigate the approximate numerical solutions for a specific class of fractional Begley-Torvik equations (FBTE) equipped with fractional integral boundary condition. Such fractional integral boundary condition allows us to understand the non-local behavior of FBTE along with the given domain. The algorithm methodology depends on creating an orthonormal basis based on reproducing kernel function that satisfies the constraint boundary conditions so that the solution is finally formulated in the form of a uniformly convergent series in $\varpi_3[a, b]$. From a numerical point of view, some illustrative examples are provided to determine the appropriateness of algorithm design and the effect of using non-classical boundary conditions on the behavior of solutions approach.

Keywords: fractional Begley-Torvik equations, integral boundary condition, reproducing kernel Hilbert space method, numerical approximation

MSC 2020: 47B32, 26A33, 34A08, 33F05, 65T50

1 Introduction

The subject of fractional differential equations (FDEs) has been employed as an effective and qualitative tool used in the formulation and modeling of complex dynamical systems and phenomena with incomprehensible behavior. This is mainly due to the fact that the fractional integrals and derivative operators provide an accurate description of the memory and hereditary properties of different systems [1–5]. Really, FDEs are more convenient and comprehensive models compared to classical differential equations models. As is well known, the Bagley-Torvik equation is among the most important equations with a prestigious position in mathematical modeling. Therefore, the objective of our work is to investigate the performance of reproducing kernel Hilbert space method (RKHSM) to solve a class of fractional Begley-Torvic equations (FBTEs) fitted with an integral boundary condition of the form:

$$\begin{cases} u''(x) + p(x)\mathcal{D}_x^{\alpha}u(x) + q(x)u(x) = \mathfrak{g}(x, u(x)), \\ u(a) = u_0, u(b) = \lambda \mathcal{I}_x^{\beta}u(b). \end{cases} \tag{1.1}$$

*** Corresponding author: Mohammed Al-Smadi,** College of Commerce and Business, Lusail University, Lusail, Qatar; Nonlinear Dynamics Research Center (NDRC), Ajman University, Ajman, UAE; Department of Applied Science, Ajloun College, Al Balqa Applied University, Ajloun, 26816, Jordan, e-mail: malsmadi@lu.edu.qa
Mazin Aljazzazi, Banan Maayah: Department of Mathematics, Faculty of Science, The University of Jordan, Amman, 11942, Jordan
Nadir Djeddi: Department of Mathematics and Computer Science, Larbi Tebessi University, Tebessa 12002, Algeria
Shaher Momani: Department of Mathematics, Faculty of Science, The University of Jordan, Amman, 11942, Jordan; Nonlinear Dynamics Research Center (NDRC), Ajman University, Ajman, UAE

For equation (1.1) to be well posed, it must be accompanied by the following assumptions: $x \in [a, b]$; u_0, and λ are the real constants, $p(x)$, $q(x)$, and $\mathfrak{g}(x, u(x))$ are the known functions; $u(x)$ is an unknown function to be determined. Here, $\mathcal{D}_x^{\alpha}$ with $1 < \alpha \leq 2$ represent the Caputo fractional derivatives and $\mathcal{I}^{\beta}$ with $1 < \beta \leq 2$ represent the Riemann-Liouville fractional integrals.

FBTE provides a high-precision mathematical model used to describe the motion of a steel plate immersed in a Newtonian fluid, which was proposed during the application of the fractional operator to viscoelastic theory by Baglay and Torvik [6–9]. On the other hand, due to the importance of FBTE in various fields of applied science and engineering, such as thermoelasticity, image processing, fluid flow, quantum and fluid physics, the numerical solutions for different classes of FBTEs involving boundary and initial constraint conditions have been extensively investigated by many researchers, and their works are attached in [10–15]. In contrast to this, except for some rare attempts, the investigation of FBTE numerical solutions subject to integral boundary conditions has not been addressed, despite the importance of constraint integral boundary conditions in modern mathematical modeling [16].

It is well known to us that classical boundary conditions cannot describe certain properties of chemical, physical, or other processes that may occur within the domain. Covering this limitation, Bicadze and Samarskii [17] introduced the concept of non-classical boundary conditions, which is a broader concept of integral boundary conditions. These conditions are used very efficiently to define changes that occur in non-local positions or fragments within a domain defined by unknown function values at endpoints or boundary of the domain. Generally, integral boundary conditions have various applications in applied fields, including underground water flow, population dynamics, blood flow problems, and chemical engineering. For more details of non-local value problems, we refer the reader to [18–22] and references cited therein.

At any rate, using a modern operational algorithm based on the reproducing kernel theory, we aim to investigate the numerical solutions of the FBTE fitted with an integral boundary condition. On other hand, in addition to the fact that the RKHSM is widely used to investigate the numerical solutions of many models related to differential-integral operators, it has the following advantages: first, the conditions for determining the solution in equation (1.1) can be imposed on the appropriate reproducing kernel Hilbert space (RKHS), and thus, a reproducing kernel function that implicitly contributes to determining the shape of the solution can be determined. Second, the numerical solutions and their derivatives converge rapidly to the exact solutions and their derivatives, respectively, Third, the RKHS algorithm is mesh-free, easily implemented, and needs no time discretization. For more details on numerical methods for fractional models, we refer the reader to [23–45].

The rest of this work is organized as follows: Section 2 is devoted to reminding some of the basic properties and concepts of fractional calculus. Section 3 is devoted to constructing two RKHSs that satisfy the constraint boundary conditions. Section 4 is devoted to explaining the working mechanism of the kernel method, as well as providing an operational algorithm that explains all the implementation steps on equation (1.1). In order to support the theoretical aspect of the RKHS method, Section 5 is devoted to numerical discussions. Finally, some concluding remarks and advice are provided in Section 6.

2 Main definitions and concepts

In this section, we are interested in reviewing some concepts and properties related to fractional calculus, which contribute to the settings and processing of equation (1.1).

Definition 2.1. [27] The Riemann-Liouville fractional integral of order α of a function $u(x)$ are described by:

$$\begin{aligned} \mathcal{I}_x^{\alpha} u(x) &= \frac{1}{\Gamma(\alpha)} \int_a^x (x - y)^{\alpha - 1} u(y) \mathrm{d}y, \alpha > 0, a \leq x \leq b; \\ \mathcal{I}_x^{0} u(x) &= u(x). \end{aligned} \tag{2.1}$$

Lemma 2.2. *For each* $\alpha, \beta \geq 0$ *and* $\gamma \geq 1$, *the following properties have been achieved*:
(1) $\mathcal{I}_x^{\alpha}\mathcal{I}_x^{\beta}u(x) = \mathcal{I}_x^{\alpha+\beta}u(x)$.
(2) $\mathcal{I}_x^{\alpha}x^{\gamma} = \frac{\Gamma(\gamma+1)}{(\alpha+\gamma+1)}x^{\alpha+\gamma}$.

The Riemann-Liouville fractional derivatives have particular drawbacks when trying to model real-world phenomena using FDEs. So, we will introduce a modified fractional differential operator suggested by Caputo.

Definition 2.3. [27] The Caputo fractional derivatives of order $m-1 \leq \alpha \leq m$ of a function $u(x)$ are described by:

$$\mathcal{D}_x^{\alpha}u(x) = \frac{1}{\Gamma(m-\alpha)}\int_a^x (x-y)^{m-\alpha-1}u^{(m)}(y)\mathrm{d}y,\ \alpha > 0,\ a \leq x \leq b. \tag{2.2}$$

Also, let us introduce one of the most important properties,

Lemma 2.4. *If* $m-1 \leq \alpha \leq m$, $m \in \mathbb{N}$, $\alpha > 0$, $x > a$, *and* $\gamma > 0$, *then*
(1) $\mathcal{D}_x^{\alpha}\mathcal{I}_x^{\alpha}u(x) = u(x)$.
(2) $\mathcal{I}_x^{\alpha}\mathcal{D}_x^{\alpha}u(x) = u(x) + \sum_{m-1}^{k=0}u^{(k)}(a)\frac{x^k}{k!}; x \geq a$.
(3) $\mathcal{D}_x^{\alpha}x^{\gamma} = \frac{\Gamma(\gamma+1)}{(\gamma-\alpha+1)}x^{\gamma-\alpha}$.

3 Reproducing kernel spaces

Before proceeding to the construction of the necessary RKHSs to formulate the normalized orthonormal function systems that control the determination of the form of the solution, it is necessary to indicate some basic concepts.

Definition 3.1. [41] Let H be a Hilbert space defined on an abstract set Ω. A function $\theta : \Omega \times \Omega \to \mathbb{C}$ is called a reproducing kernel of H if it satisfies the two following conditions:
(1) For each $x \in \Omega$, $\theta(\cdot, x) \in H$,
(2) For each $u \in H$ and $x \in \Omega$, $\langle u(\cdot), \theta(\cdot, x)\rangle_H = u(x)$.
"The reproducing property." The reproducing property condition is one of the properties resulting from the direct application of Riesz representation theorem to Hilbert space.

Indeed, a Hilbert space H that possesses a reproducing kernel function is called a reproducing kernel Hilbert space (RKHS). Along with this analysis, we denote $\|u\|_H = \langle u(x), u(x)\rangle_H$, for $u(x) \in H$ and $H \in \{\varpi_1, \varpi_3\}$. However, $AC[a, b]$ is the set of functions that is absolutely continuous on $[a, b]$.

Definition 3.2. [41] The Hilbert space $\varpi_1[a, b]$ is defined as follows:

$$\varpi_1[a, b] = \{u = u(x) : u \in AC[a, b], u' \in L^2[a, b]\},$$

while the inner product is given as:

$$\langle u, v\rangle_{\varpi_1} = u(a)v(a) + \int_a^b u'(x)v'(x)\mathrm{d}x,\ u, v \in \varpi_1[a, b]. \tag{3.1}$$

In [41], the authors have proved that $\varpi_1[a, b]$ is a complete RKHS and its reproducing kernel function is given as follows:

$$R_x(y) = \frac{1}{2\sinh(b-a)}[\cosh(x+y-b-a) + \cosh(|x-y|-b+a)]. \tag{3.2}$$

Now, we construct a RKHS $\varpi_3[a,b]$ in which every function satisfies the boundary conditions $u(a) = 0$ and $u(b) = \lambda \mathcal{I}_x^{\beta} u(b)$.

Definition 3.3. [29] The Hilbert space $\varpi_3[a,b]$ is defined as follows:

$$\varpi_3[a,b] = \{u = u(x) : u^{(i)} \in AC[a,b], i = 0,1,2; u^{(3)} \in L^2[a,b], u(a) = 0, u(b) = \lambda \mathcal{I}_x^{\beta} u(b)\}.$$

This space is equipped with the following inner product:

$$\langle u, v\rangle_{\varpi_3} = \sum_{i=0}^{2} u^{(i)}(a)v^{(i)}(a) + \int_a^b u^{(3)}(x)v^{(3)}(x)\mathrm{d}x,\ u, v \in \varpi_3[a,b]. \tag{3.3}$$

Theorem 3.4. *The space $\varpi_3[a,b]$ is a complete RKHS, i.e., for each $x \in [a,b]$, there exists a reproducing kernel $k_x(y) \in \varpi_3[a,b]$ such that $\langle u(y), k_x(y)\rangle_{\varpi_3} = u(x)$ for each $u(x) \in \varpi_3[a,b]$. The reproducing kernel is given as*:

$$K_x(y) = \begin{cases} \sum_{k=1}^{6} a_k(x)y^{k-1} - cG(y), & y < x; \\ \sum_{k=1}^{6} b_k(x)y^{k-1} - cG(y), & x \le y, \end{cases} \tag{3.4}$$

where $G(y) = \int_a^y\int_a^y\int_a^y\int_a^y\int_a^y\int_a^y \frac{\lambda}{\Gamma(\beta)(b-y)^{1-\beta}}\mathrm{d}y\mathrm{d}y\mathrm{d}y\mathrm{d}y\mathrm{d}y\mathrm{d}y$. Here, $a_k(x)$, $b_k(x)$, and c are the unknown coefficients of $k_x(y)$.

Proof. This proof consists of two main parts: the first part is dedicated to providing completeness and reproducing property of the Hilbert space $\varpi_3[a,b]$, and we find it in detail in [29]. Second, in order to determine the expression form of the reproducing kernel function $K_x(y)$ in $\varpi_3[a,b]$, we perform the following steps:

Through diverse integration by parts for (3.3), we have

$$\begin{aligned} \langle u(y), K_x(y)\rangle_{\varpi_3} = &\sum_{k=0}^{2} u^{(k)}(a)[\partial_y^k K_x(a) - (-1)^{2-k}\partial_y^{5-k} K_x(a)] \\ &+ \sum_{k=0}^{2}(-1)^{2-k}u^{(k)}(b) - \int_a^b u(y)\partial_y^6 K_x(y)\mathrm{d}y. \end{aligned} \tag{3.5}$$

Since $u(x) \in \varpi_3[a,b]$, it follows that $u(a) = 0$ and $u(b) = \lambda \mathcal{I}_x^{\beta} u(b)$.

Then, we have

$$\begin{aligned} \langle u(y), K_x(y)\rangle_{\varpi_3} = &\sum_{k=1}^{2} u^{(k)}(a)[\partial_y^k K_x(a) - (-1)^{2-k}\partial_y^{5-k} K_x(a)] + \sum_{k=0}^{2}(-1)^{2-k}u^{(k)}(b) \\ &- \int_a^b u(y)\partial_y^6 K_x(y)\mathrm{d}y + c(u(b) - \lambda \mathcal{I}_x^{\beta} u(b)) \end{aligned} \tag{3.6}$$

if

$$\begin{cases} \partial_y^1 K_x(a) + \partial_y^4 K_x(a) = 0; \\ \partial_y^2 K_x(a) + \partial_y^3 K_x(a) = 0; \\ \partial_y^3 K_x(b) = 0; \\ \partial_y^4 K_x(b) = 0; \\ \partial_y^5 K_x(b) + c = 0. \end{cases} \tag{3.7}$$

Also, since $k_x(y) \in \varpi_3[a, b]$, we can obtain

$$k_x(a) = 0 \quad \text{and} \quad k_x(b) = \lambda \mathcal{I}_x^{\beta} k_x(b). \tag{3.8}$$

From equations (3.7) and (3.8), equation (3.5) implies

$$\langle u(y), K_x(y) \rangle_{\varpi_3} = -\int_a^b u(y) \left[\partial_y^6 K_x(y) + \frac{c\lambda}{\Gamma(\beta)} \frac{1}{(b-y)^{1-\beta}} \right] \mathrm{d}y. \tag{3.9}$$

For any $x \in [a, b]$, if $k_x(y)$ satisfies

$$\partial_y^6 K_x(y) + \frac{c\lambda}{\Gamma(\beta)} \frac{1}{(b-y)^{1-\beta}} = -\delta(y - x), \tag{3.10}$$

then

$$\langle u(y), K_x(y) \rangle_{\varpi_3} = u(x). \tag{3.11}$$

When $y \neq x$, the corresponding characteristic equation of equation (3.10) is given by:

$$r^6 = 0.$$

Thus, we obtain the characteristic value $r = 0$ whose order multiplicity is 6. So, let

$$K_x(y) = \begin{cases} \sum_{k=1}^{6} a_k(x) y^{k-1} - cG(y), & y < x, \\ \sum_{k=1}^{6} b_k(x) y^{k-1} - cG(y), & x \leq y, \end{cases} \tag{3.12}$$

where $G(y) = \int_a^y \int_a^y \int_a^y \int_a^y \int_a^y \int_a^y \frac{\lambda}{\Gamma(\beta)(b-y)^{1-\beta}} \mathrm{d}y\mathrm{d}y\mathrm{d}y\mathrm{d}y\mathrm{d}y\mathrm{d}y$.

Furthermore, let $K_x(y)$ satisfy

$$\lim_{y \to x^-} \partial_y^k K_x(y) = \lim_{y \to x^+} \partial_y^k K_x(y), \; i = 0, 1, \ldots, 4. \tag{3.13}$$

Integrating equation (3.10) from $x - \varepsilon$ to $x + \varepsilon$ with respect to y and letting $\varepsilon \to 0$, we have the jump degree of $\partial_y^5 K_x(y)$ at $y = x$:

$$\lim_{y \to x^-} \partial_y^5 K_x(y) - \lim_{y \to x^+} \partial_y^5 K_x(y) = 1. \tag{3.14}$$

From equations (3.7) and (3.13)–(3.14), the unknown coefficients a_k, b_k, $k = 1, 2, \ldots, 6$, and c in equation (3.12), can be acquired and $K_x(y)$ in equation (3.12) fulfill equation (3.11). □

4 Implementation of the method

In this section, we seek to construct an orthonormal function system $\{\overline{\psi}_i(x)\}_{i=1}^{\infty}$ of $\varpi_3[a, b]$ using the well-known Gram-Schmidt orthogonalization process. The creation of this basis contributes to a large extent in

representing the formula of the approximate and analytical solution to FBTE. In order to investigate this, let us first begin by introducing a corresponding linear operator Q as:

$$\begin{cases} Q : \varpi_3[a,b] \longrightarrow \varpi_1[a,b], \\ Qu(x) = u''(x) + p(x)\mathcal{D}_x^q u(x) + q(x)u(x). \end{cases} \tag{4.1}$$

Thus, based on this, the corresponding form of FBTE can be reformulated as follows:

$$\begin{cases} Qu(x) = \mathfrak{g}(x, u(x)), \\ u(a) = 0, u(b) = \lambda \mathcal{I}_x^\beta u(b), \end{cases} \tag{4.2}$$

where $u(x) \in \varpi_3[a,b]$ and $\mathfrak{g}(x,u(x)) \in \varpi_1[a,b]$.

It should be noted that with the use of the functional properties and also the reproducing property, we can easily prove that the operator Q is linear and bounded.

Next, we construct the orthonormal function system $\{\overline{\psi}_i(x)\}_{i=1}^\infty$ of $\varpi_3[a,b]$ as follows: pic out $\{x_i\}_{i=1}^\infty$ as a countable dense subset on $[a,b]$; set $\varphi_i(x) = R_{x_i}(x)$ and define $\psi_i(x) = Q^\star\varphi_i(x)$, $i = 1,2,\ldots$, where $Q^\star$ is the conjugate operator of Q. Thus, in terms of the reproducing property of RKHS $\varpi_1[a,b]$, it follows that

$$\langle u(x), \psi_i(x)\rangle_{\varpi_3} = \langle u(x), Q^\star\varphi_i(x)\rangle_{\varpi_3} = \langle Qu(x), \varphi_i(x)\rangle_{\varpi_1} = Qu(x_i); i = 1,2,\ldots.$$

As the same concept, from the reproducing property of RKHS $\varpi_3[a,b]$, it follows that

$$\psi_i(x) = \langle \psi_i(y), K_{x_i}(y)\rangle_{\varpi_3} = \langle Q^\star\varphi_i(x), K_{x_i}(y)\rangle_{\varpi_3} = \langle \varphi_i(x), QK_{x_i}(y)\rangle_{\varpi_1} = QK_{x_i}(y)|_{y=x_i}.$$

The orthonormal functions system $\{\overline{\psi}_i(t)\}_{i=1}^\infty$ of $\varpi_3[a,b]$ is constructed using the well-known Gram-Schmidt orthogonalization process on $\{\psi_i(x)\}_{i=1}^\infty$ as follows:

$$\overline{\psi}_i(x) = \sum_{k=1}^{i} \varrho_{ik}\psi_k(x), \varrho_{ii} > 0, i = 1,2,\ldots, \tag{4.3}$$

where the coefficient of orthogonalization ϱ_{ik} is obtained using the following steps presented in Algorithm 1:

Algorithm 1: Applying the Gram-Schmidt orthogonalization process for obtaining ϱ_{ik} and $\{\overline{\psi}_i(t)\}_{i=1}^\infty$

---

procedure: DO THE NEXT STEPS TO OBTAIN $\{\overline{\psi}_i(t)\}_{i=1}^\infty$ of $\varpi_3[a,b]$.

Phase I:

for $i = 1$ to n and $k = 1$ to i **do**

$$\varrho_{ik}\,|_{i=k=1} = \frac{1}{\|\psi_i(x)\|_{\varpi_3[a,b]}},$$

$$\varrho_{ik}\,|_{i=k\neq 1} = \frac{1}{\|\psi_i(x)\|_{\varpi_3[a,b]} - \sum_{p=1}^{i-1}\langle \psi_i(x), \overline{\psi}_{ip}(x)\rangle_{\varpi_3[a,b]}},$$

$$\varrho_{ik}\,|_{i>k} = -\frac{1}{\sqrt{\|\psi_i(x)\|_{\varpi_3[a,b]} - \sum_{p=1}^{i-1}\langle \psi_i(x), \overline{\psi}_{ip}(x)\rangle^2_{\varpi_3[a,b]}}}\sum_{p=k}^{i-1}\langle \psi_i(x), \overline{\psi}_{ip}(x)\rangle_{\varpi_3[a,b]}\varrho_{pk},$$

Output: The orthogonalization coefficients ϱ_{ik}.

Phase II:

for $i = 1$ to n **do**

$\overline{\psi}_i(x) = \sum_{k=1}^{i}\varrho_{ik}\psi_i(x)$.

Output: systems of orthonormal functions $\{\overline{\psi}_i(x)\}_{i=1}^\infty$.

Lemma 4.1. *Under the previous assumptions, if* $\{x_i\}_{i=1}^\infty$ *is a countable dense set on* $[a,b]$, *then* $\{\psi_i(x)\}_{i=1}^\infty$ *is a complete function system of* $\varpi_3[a,b]$.

Proof. For each $u(x) \in \varpi_3[a,b]$, if $\langle u(x), \psi_i(x)\rangle_{\varpi_3} = 0$, $i = 1,2,\ldots$, then

$$\langle u(x), \psi_i(x)\rangle_{\varpi_3} = \langle u(x), Q^{*}\varphi_i(x)\rangle_{\varpi_3} = \langle Qu(x), \varphi_i(x)\rangle_{\varpi_3} = Qu(x_i) = 0. \tag{4.4}$$

Since $\{x_i\}_{i=1}^{\infty}$ is a countable dense set on $[a, b]$, then $Qu(x) = 0$ and $u(x) = 0$ by the existence of the inverse operator Q^{-1} of Q. So, $\{\psi_i(x)\}_{i=1}^{\infty}$ is the complete function system of $\varpi_3[a, b]$. □

Lemma 4.2. *Suppose that $u(x)$ is the solution of equation* (4.2)*, then $u(x)$ fulfills the following equations*:

$$\langle u(\cdot), \psi_i(\cdot)\rangle_{\varpi_3} = \mathfrak{g}(x_i, u(x_i)); i = 1, 2, \ldots, \tag{4.5}$$

where $\{x_i\}_{i=1}^{\infty}$ is a countable dense set on $[a, b]$.

Proof. Since $u(x)$ is the solution of equation (4.2), then $Qu(x) = \mathfrak{g}(x, u(x))$ and

$$\langle u(\cdot), \psi_i(\cdot)\rangle_{\varpi_3} = \langle Qu(\cdot), \varphi_i(\cdot)\rangle_{\varpi_1} = Qu(x_i) = \mathfrak{g}(x_i, u(x_i)); i = 1, 2, \ldots. \tag{4.6}$$

□

Theorem 4.3. *If $u(x) \in \varpi_3[a, b]$ is the exact solution of equation* (4.2)*, then $u(x)$ can be represented as follows*:

$$u(x) = Q^{-1}\mathfrak{g}(x, u(x)) = \sum_{i=1}^{\infty} B_i \overline{\psi}_i(x), \tag{4.7}$$

where $B_i = \sum_{k=1}^{i} \varrho_{ik}\mathfrak{g}(x_k, u(x_k))$.

Proof. $u(x)$ can be expanded in terms of the Fourier series expansion:

$$\begin{aligned} u(x) &= \sum_{i=1}^{\infty} \langle u(x), \overline{\psi}_i(x)\rangle_{\varpi_3} \overline{\psi}_i(x) \\ &= \sum_{i=1}^{\infty}\sum_{k=1}^{i} \varrho_{ik}\langle u(x), \psi_i(x)\rangle_{\varpi_3} \overline{\psi}_i(x) \\ &= \sum_{i=1}^{\infty}\sum_{k=1}^{i} \varrho_{ik}\langle u(x), Q^{*}\varphi_k(x)\rangle_{\varpi_3} \overline{\psi}_i(x) \\ &= \sum_{i=1}^{\infty}\sum_{k=1}^{i} \varrho_{ik}\langle Qu(x), \varphi_k(x)\rangle_{\varpi_1} \overline{\psi}_i(x) \\ &= \sum_{i=1}^{\infty}\sum_{k=1}^{i} \varrho_{ik}\mathfrak{g}(x_k, u(x_k))\overline{\psi}_i(x). \end{aligned} \tag{4.8}$$

The representation of the n-term approximation solution $u_n(x)$ to $u(x)$ can be acquired using truncating formula (4.7) as follows:

$$u_n(x) = \sum_{i=1}^{n}\sum_{k=1}^{i} \varrho_{ik}\mathfrak{g}(x_k, u(x_k))\overline{\psi}_i(x). \tag{4.9}$$

Since $\varpi_3[a, b]$ is a Hilbert space, $\sum_{i=1}^{\infty} B_i\overline{\psi}_i(x)$ is finite.

Therefore, the sequence $u_n(x)$ is convergent in the sense of the norm $\varpi_3[a, b]$. Take $\Pi = \overline{\mathrm{Span}\{\overline{\psi}_i(x)\}_{i=0}^{n}}$; thus, $\Pi \subseteq \varpi_3[a, b]$, i.e., $u_n(x)$ is the projection of exact solution $u_n(x)$ onto Π.

It is worth noting here that if equation (4.2) is linear, i.e., $\mathfrak{g}(x_k, u(x_k)) = \mathfrak{g}(x_k)$, then the exact and approximate solutions can be acquired directly from equations (4.8) and (4.9), respectively. Otherwise, the approximate solution of equation (4.2) can be obtained using the following iterative formula:

$$\begin{cases} u_0(x) = 0, \\ u_m(x) = \sum_{i=1}^{m} B_i\overline{\psi}_i(x), \end{cases} \tag{4.10}$$

where $B_i = \sum_{k=1}^{i} \varrho_{ik}\mathfrak{g}(x_k, u_{k-1}(x_k))$. □

According to the aforementioned method, we will give the following algorithm as well as summarize its procedure for finding the approximate solution to equation (4.2).

Algorithm 2: Finding the approximate solution $u_n(x)$ of $u(x)$ in FBTE (1.1).

procedure:

Phase I: Construct an appropriate reproducing kernel function $K_x(y)$ that satisfies the constraint boundary conditions of the equation (1.1).

Phase II: Pick out any countable dense $\{x_i\}_{i=1}^{n}$ subset of the interval [a,b].

Phase III: Set the complete function system as:

$\psi_i(x) = Q_y K_x(y)|_{y=x_i}$. $i = 1, 2, \ldots, n$.

Phase IV: Take out the orthogonalization coefficients ϱ_{ik}.

Phase V:

A. Pick out any initial data $u_0(x_1)$.

B. Put $u(x_1) = u_0(x_1)$.

C. begin with $i = 1$ to obtain that $B_1 = \varrho_{11}\mathfrak{g}(x_1, u_0(x_1))$, $u_1(x) = B_1\overline{\psi}_1(x)$.

Phase VI:

for $i = 1$ to n **do**, the following substeps:

A. Set $m = i + 1$, and set

$B_m = \sum_{k=1}^{m}\varrho_{ik}\mathfrak{g}(x_k, u_{m-1}(x_k))$;

$u_m(x) = \sum_{i=1}^{m}B_i\overline{\psi}_i(x)$.

B. Save the setting values of $u_m(x)$, and implement the next step:

C. If $m > n$; then **Stop**. Else, let $i = m$ and go to step A in this subroutine.

5 Computational experiments

To demonstrate the robustness and suitability of the analytical approach presented in this study, we conduct a detailed and integrated numerical discussion of some illustrative applications.

We include the results and numerical data obtained with Mathematica 12.0 software package in the form of tables and graphs.

Example 5.1. Consider the following FBTE with a fitted integral boundary condition:

$$\begin{aligned} u''(x) + \sqrt{\pi}x^2\mathcal{D}_x^{\frac{3}{2}}u(x) + \left(1 - 4x^{\frac{1}{2}}\right) &= x^2 + 1, \\ u(0) = 0, u\left(\frac{1}{10}\right) &= \frac{525\sqrt{10\pi}}{16}\mathcal{I}_x^{\beta}u\left(\frac{1}{10}\right), \end{aligned} \tag{5.1}$$

where $x \in \left[0, \frac{1}{10}\right]$, $\lambda = \frac{525\sqrt{10\pi}}{16}$. When $\beta = \frac{3}{2}$, the exact solution of equation (5.1) can be given as: $u(x) = x^2$.

Taking $x_i = \frac{i-1}{n-1}$, $i = 1, \ldots, n$ and n=11, the implementation of the proposed algorithm on Example 5.1 allows us to obtain the embedded numerical data in the form of tables and graphs, which we display as follows:

Table 1 displays the absolute errors and the relative errors of approximate solutions at some selected grid points in $\left[0, \frac{1}{10}\right]$ when $(\alpha, \beta) = \left(\frac{3}{2}, \frac{3}{2}\right)$. Also, in order to demonstrate the safety and appropriateness of the results obtained using the proposed method, we conducted a comparative study between the absolute error available

to us using our method at $(\alpha, \beta) = \left(\frac{3}{2}, \frac{3}{2}\right)$ and the one obtained using the generalized piecewise Taylor-series expansion method (GPTSE), taking into account the effect of the fractional parameter as shown in analysis [16]. The results of this comparison are listed in Table 2.

Exclusively, Figure 1 represents the graphical translation of Table 1 data, which enables us to show the extent to which the approximate and exact solution behavior agrees. On the other hand, Figure 2 shows the effect of changing the parameter β on the behavior of the approximate solutions, and this is mainly due to the close relationship between the form of the solution and the constraint boundary conditions of FBTE.

Example 5.2. Consider the following FBTE fitted with an integral boundary condition:

$$\begin{aligned} &u''(x) - 5\pi x \mathcal{D}_x^{\frac{1}{2}} u(x) + 16x^{\frac{1}{2}} u(x) = 6x, \\ &u(0) = 0, u\left(\frac{1}{10}\right) = \frac{35\sqrt{10\pi}}{32} \mathcal{I}_x^{\beta} u\left(\frac{1}{10}\right), \end{aligned} \tag{5.2}$$

where $x \in \left[0, \frac{1}{10}\right]$ and $\lambda = \frac{35\sqrt{10\pi}}{32}$. It can be calculated that when $\beta = \frac{1}{2}$, the exact solution of equation (5.2) is as follows: $u(x) = x^3$.

Taking $x_i = \frac{i-1}{n-1}$, $i = 1, \ldots, n$ and $n = 11$, the implementation of the proposed algorithm on Example 5.2 allows us to obtain the embedded numerical data in the form of tables and graphs, which we display as follows:

Table 3 displays the absolute errors and the relative errors of approximate solutions at some selected grid points in $\left[0, \frac{1}{10}\right]$ when $(\alpha, \beta) = \left(\frac{1}{2}, \frac{1}{2}\right)$. Exclusively, Figure 3 represents the graphical translation of Table 3 data, which enables us to show the extent to which the approximate and exact solution behavior agrees. On the other hand, Figure 4 shows the effect of changing the parameter β on the behavior of the approximate solutions.

Example 5.3. Consider the following FBTE fitted with an integral boundary condition:

$$\begin{aligned} &u''(x) + \Gamma(3-\alpha) \mathcal{D}_x^{\alpha} u(x) - 2u(x) = 2, \\ &u(0) = 0, u(1) = \frac{\Gamma(3+\beta)}{2} \mathcal{I}_x^{\beta} u(1), \end{aligned} \tag{5.3}$$

where $x \in [0, 1]$ and $\lambda = \frac{\Gamma(3+\beta)}{2}$. It can be calculated that when $(\alpha, \beta) = (\frac{1}{2}, \frac{1}{2})$, the exact solution of equation (5.3) is: $u(x) = x^2$.

Taking $x_i = \frac{i-1}{n-1}$, $i = 1, \ldots, n$ and $n = 11$, the numerical results for Example 5.3 are shown in Table 4.

Table 1: Numerical results for Example 5.1 when $\beta = \frac{3}{2}$ and $n = 11$

x	Exact sol. $u(x)$	Approximate sol. $u_{11}(x)$	$\lvert u(x) - u_{11}(x) \rvert$	$\lvert u(x) - u_{11}(x) \rvert / \lvert u(x) \rvert$
0.01	0.0001	0.0001	4.4345×10^{-16}	4.4345×10^{-12}
0.02	0.0004	0.0004	8.9284×10^{-16}	2.2321×10^{-12}
0.03	0.0009	0.0009	1.3981×10^{-15}	1.5534×10^{-12}
0.04	0.0016	0.0016	2.0914×10^{-15}	1.3071×10^{-12}
0.05	0.0025	0.0025	2.8649×10^{-15}	1.1459×10^{-12}
0.06	0.0036	0.0036	3.7318×10^{-15}	1.0366×10^{-12}
0.07	0.0049	0.0049	5.1903×10^{-15}	1.0592×10^{-12}
0.08	0.0064	0.0064	5.7992×10^{-15}	9.0612×10^{-13}
0.09	0.0081	0.0081	7.1991×10^{-15}	8.8878×10^{-13}
0.10	0.0100	0.0100	1.1050×10^{-14}	1.1050×10^{-12}

Table 2: Numerical comparison of absolute errors for Example 5.1

x	GPTSE [16] for $(m, n) = (8, 1)$ and $\beta = \frac{3}{2}$			Present method
	$\gamma = 1$	$\gamma = 3/4$	$\gamma = 1/2$	$n = 11$
0.01	1.7619×10^{-10}	5.9296×10^{-10}	3.3359×10^{-9}	4.4345×10^{-16}
0.02	1.4548×10^{-10}	3.8592×10^{-9}	6.6717×10^{-8}	8.9284×10^{-16}
0.03	2.2558×10^{-11}	5.7885×10^{-10}	1.0007×10^{-9}	1.3981×10^{-15}
0.04	3.0163×10^{-11}	7.7170×10^{-10}	1.3343×10^{-9}	2.0914×10^{-15}
0.05	4.2202×10^{-10}	9.6439×10^{-9}	1.6678×10^{-8}	2.8649×10^{-15}
0.06	5.1368×10^{-10}	1.2873×10^{-8}	2.2330×10^{-8}	3.7318×10^{-15}
0.07	8.4269×10^{-10}	1.3412×10^{-9}	2.3613×10^{-8}	5.1903×10^{-15}
0.08	1.5038×10^{-10}	1.3250×10^{-9}	2.3327×10^{-8}	5.7992×10^{-15}
0.09	9.4843×10^{-10}	1.2620×10^{-9}	2.1811×10^{-8}	7.1991×10^{-15}
0.10	2.1213×10^{-10}	1.1645×10^{-9}	1.9234×10^{-9}	1.1050×10^{-14}

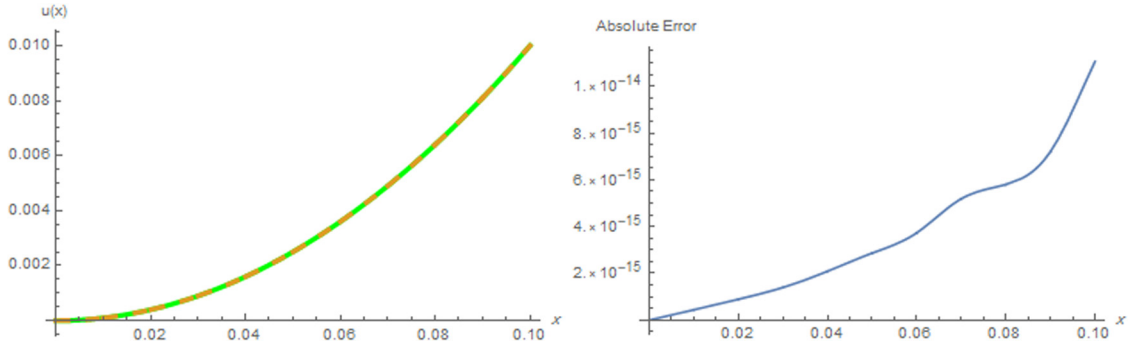

Figure 1: Congruent figure of $u(x)$ with $u_{11}(x)$ and the $|u(x) - u_{11}(x)|$ for Example 5.1.

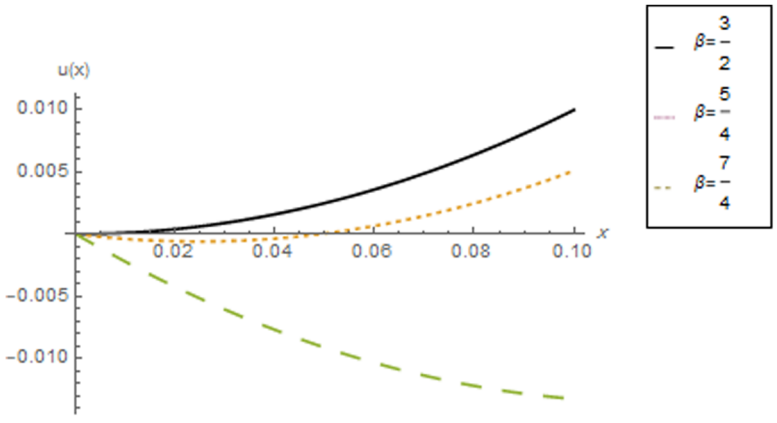

Figure 2: Approximate solutions for Example 5.1 with $\beta \in \{\frac{5}{4}, \frac{3}{2}, \frac{7}{4}\}$.

Table 4 shows the leverage of changing the parameter β on the behavior of absolute errors when fixing $\alpha = 1/2$. This is mainly due to the fact that any perturbation about the level of the constraint boundary conditions leads to a change in the formula of $K_x(y)$, which, in turn, enters into the formulation of the approximate solution $u_n(x)$.

Table 3: Numerical results for Example 5.2 when $\beta = \frac{3}{2}$ and $n = 11$

x	Exact sol. $u(x)$	Approximate sol. $u_{11}(x)$	$\lvert u(x)-u_{11}(x)\rvert$	$\lvert u(x)-u_{11}(x)\rvert/\lvert u(x)\rvert$
0.01	0.000001	0.000001	1.5496×10^{-9}	1.552×10^{-3}
0.02	0.000008	0.000008	2.8839×10^{-9}	3.6062×10^{-4}
0.03	0.000027	0.000027	2.7783×10^{-9}	1.0291×10^{-4}
0.04	0.000064	0.000064	7.8343×10^{-10}	1.2241×10^{-5}
0.05	0.000125	0.000125	9.7371×10^{-9}	7.7891×10^{-5}
0.06	0.000216	0.000216	2.5151×10^{-8}	1.1642×10^{-4}
0.07	0.000343	0.000343	4.6832×10^{-8}	1.3652×10^{-4}
0.08	0.000512	0.000512	7.3396×10^{-8}	1.4333×10^{-4}
0.09	0.000729	0.000729	1.0275×10^{-7}	1.4093×10^{-4}
0.10	0.001000	0.001000	1.3285×10^{-7}	1.3282×10^{-4}

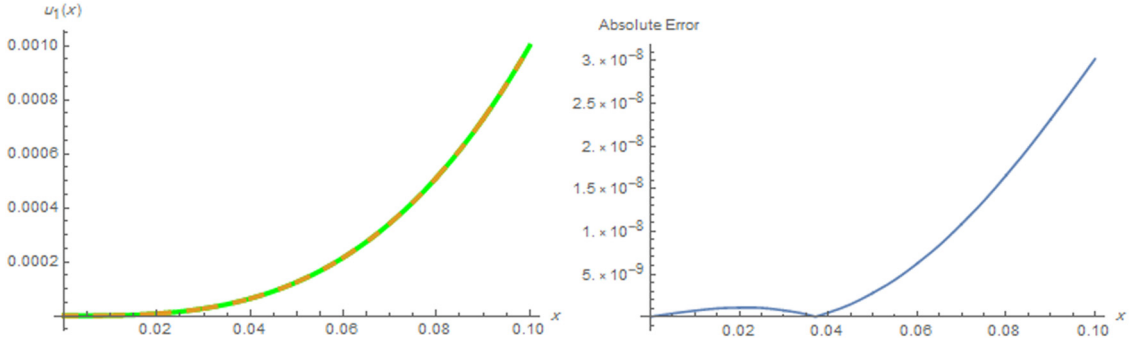

Figure 3: Congruent figure of $u(x)$ with $u_{11}(x)$ and the $|u(x) - u_{11}(x)|$ for Example 5.2.

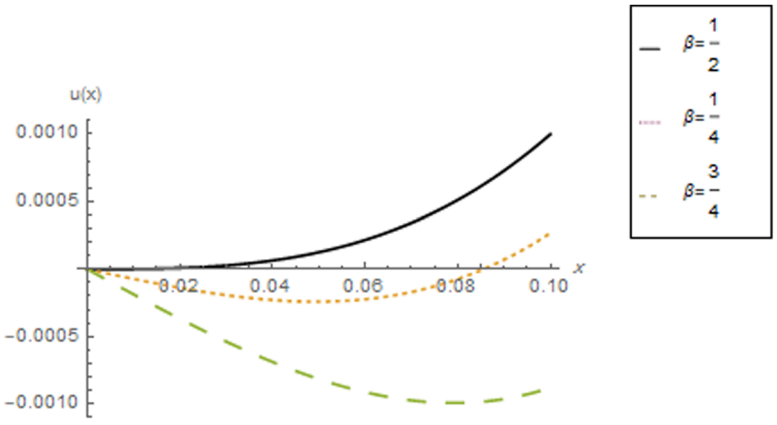

Figure 4: Approximate solutions for Example 5.2 with $\beta \in \{\frac{1}{4}, \frac{1}{2}, \frac{3}{4}\}$.

6 Conclusion

The main purpose of the current work is to propose a reliable operational algorithm based on the reproducing kernel theory. Approximate and numerical solutions for FBTEs fitted with an integral boundary condition were obtained based on a complete orthogonal system in Hilbert spaces. To ensure the credibility and reliability of the proposed algorithm, a comparative study of some illustrative examples was carried out, in which the obtained results were compared with the exact solutions and the results of some advanced methods

Table 4: Absolute errors of approximate and exact solutions of Example 5.3

x	$\lvert u(x)-u_n(x)\rvert$ for $\alpha = 1/2$, $n = 11$ and β			
	$\beta = 1/4$	$\beta = 1/3$	$\beta = 1/2$	$\beta = 3/4$
0.1	1.7347×10^{-17}	1.0408×10^{-17}	1.7347×10^{-18}	8.6736×10^{-18}
0.2	2.0817×10^{-17}	2.0817×10^{-17}	0	2.0817×10^{-17}
0.3	6.9389×10^{-17}	2.7756×10^{-17}	0	2.7755×10^{-17}
0.4	8.3267×10^{-17}	2.7756×10^{-17}	0	2.7755×10^{-17}
0.5	8.3267×10^{-17}	5.5511×10^{-17}	0	0
0.6	1.6657×10^{-16}	5.5511×10^{-17}	0	5.5511×10^{-17}
0.7	2.2204×10^{-16}	5.5511×10^{-17}	0	5.5511×10^{-17}
0.8	1.1102×10^{-16}	1.1102×10^{-16}	0	1.1102×10^{-16}
0.9	0.	1.1102×10^{-16}	0	1.1102×10^{-16}
1.	3.3307×10^{-16}	2.2204×10^{-16}	1.11022×10^{-16}	0

available. From the graphical representations, it can be seen that the behavior of the obtained solutions is consistent with each other for different fractional orders and harmonious with the integer order. On the other hand, the acquired results and numerical data reveal the accuracy, performance, and comprehensiveness of the proposed method for obtaining qualitative solutions with less effort. Therefore, we conclude that the results of this work can be exploited to find solutions for similar models fitted with non-classical boundary conditions. In future work, the current algorithm can be employed to find numerical solutions to multidimensional fractional evolution models in terms of non-local fractional derivatives.

Acknowledgement: The authors express their thanks to unknown referees for the careful reading and helpful comments.

Funding information: The authors state that no funding is involved.

Author contributions: All authors contributed equally to this article. They read and approved the final manuscript.

Conflict of interest: The authors state no conflict of interest.

Data availability statement: No data to be declared.

References

[1] A. A. Kilbas, H. M. Srivastava, and J. J. Trujillo, *Theory and Applications of Fractional Differential Equations*, in: North-Holland Mathematics Studies, vol. 204, Elsevier Science B.V., Amsterdam, 2006.

[2] P. Veeresha, D. G. Prakasha, and S. Kumar, *A fractional model for propagation of classical optical solitons by using nonsingular derivative*, Math. Methods Appl. Sci. (2020), 1–15, DOI: https://doi.org/10.1002/mma.6335.

[3] S. Kumar, *A new fractional modeling arising in engineering sciences and its analytical approximate solution*, Alex. Eng. J. **52** (2013), no. 4, 813–819.

[4] I. Podlubny, *Fractional Differential Equations*, Academic Press, San Diego, 1999.

[5] K. Diethelm, *The Analysis of Fractional Differential Equations*, Springer-Verlag, Berlin, 2010, DOI: https://doi.org/10.1007/978-3-642-14574-2.

[6] S. Abbas, M. Benchohra, J. E. Lazreg, J. J. Nieto, and Y. Zhou, *Fractional Differential Equations and Inclusions, Classical and Advanced Topics*, vol. 10, World Scientific, Hackensack, USA, 2023, p. 328, DOI: https://doi.org/10.1142/12993.

[7] Y. Yan and S. Luo, *Local polynomial smoother for solving Bagley-Torvik fractional differential equations*, Preprints, (2016), 2016080231. DOI: https://doi.org/10.20944/preprints201608.0231.v1.
[8] Y. Çenesiz, Y. Keskin, and A. Kurnaz, *The solution of the Bagley-Torvik equation with the generalized Taylor collocation method*, J. Franklin Inst. **347** (2010), 452–466.
[9] S. Yuzbasi, *Numerical solution of the Bagley-Torvik equation by the Bessel collocation method*, Math. Methods Appl. Sci. **36** (2013), 300–312.
[10] S. Kumar, A. Kumar, B. Samet, J. F. Gomez-Aguilar, and M. S. Osman, *A chaos study of tumor and effector cells in fractional tumor-immune model for cancer treatment*, Chaos Solitons Fractals **141** (2021), 110321, DOI: https://doi.org/10.1016/j.chaos.2020.110321.
[11] A. Arikoglu and A. L. Ozkol, *Solution of fractional differential equations by using differential transform method*, Chaos Solitons Fractals **34** (2017), 1473–1481.
[12] H. Mohammadi, S. Kumar, S. Rezapour, and S. Etemad, *A theoretical study of the Caputo-Fabrizio fractional modeling for hearing loss due to Mumps virus with optimal control*, Chaos Solitons Fractals **144** (2021), 110668, DOI: https://doi.org/10.1016/j.chaos.2021.110668.
[13] F. Mohammadi and S. T. Mohyud-Din, *A fractional-order Legendre collocation method for solving the Bagley-Torvik equations*, Adv. Differential Equations **2016** (2016), 269, DOI: https://doi.org/10.1186/s13662-016-0989-x
[14] S. Hasan, N. Djeddi, M. Al-Smadi, S. Al-Omari, S. Momani, and A. Fulga, *Numerical solvability of generalized Bagley-Torvik fractional models under Caputo-Fabrizio derivative*, Adv. Differential Equations **2021** (2021), 469, DOI: https://doi.org/10.1186/s13662-021-03628-x.
[15] O. Abu Arqub and B. Maayah, *Solutions of Bagley-Torvik and Painleve equations of fractional order using iterative reproducing kernel algorithm with error estimates*, Neural Comput. Appl. **29** (2016), 1465–1479.
[16] X. Zhong, X. Liu, and S. Liao, *On a generalized Bagley-Torvik equation with a fractional integral boundary condition*, Int. J. Appl. Comput. Math. **3** (2017), 727–746.
[17] A. V. Bicadze and A. A. Samarskii, *Some elementary generalizations of linear elliptic boundary value problems*, Dokl. Akad. Nauk **185** (1969), 739–740.
[18] J. Andres, *A four-point boundary value problem for the second-order ordinary differential equations*, Arch. Math. **53** (1989), 384–389.
[19] P. W. Eloe and B. Ahmad, *Positive solutions of a nonlinear nth order boundary value problem with nonlocal conditions*, Appl. Math. Lett. **18** (2005), 521–527.
[20] J. R. L. Webb and G. Infante, *Positive solutions of nonlocal boundary value problems: A unified approach*, J. Lond. Math. Soc. **74** (2006), 673–693.
[21] H. Khalil, M. Al-Smadi, K. Moaddy, R. A. Khan, and I. Hashim, *Toward the approximate solution for fractional order nonlinear mixed derivative and nonlocal boundary value problems*, Discrete Dyn. Nat. Soc. **2016** (2016), 5601821, DOI: https://doi.org/10.1155/2016/5601821.
[22] G. Gumah, M. F. M. Naser, M. Al-Smadi, S. K. Q. Al-Omari, and D. Baleanu, *Numerical solutions of hybrid fuzzy differential equations in a Hilbert space*, Appl. Numer. Math. **151** (2020), 402–412, DOI: https://doi.org/10.1016/j.apnum.2020.01.008.
[23] M. Al-Smadi, *Simplified iterative reproducing kernel method for handling time-fractional BVPs with error estimation*, Ain Shams Eng. J. **9** (2018), no. 4, 2517–2525, DOI: https://doi.org/10.1016/j.asej.2017.04.006.
[24] M. Al-Smadi, O. Abu Arqub, and S. Momani, *Numerical computations of coupled fractional resonant Schrödinger equations arising in quantum mechanics under conformable fractional derivative sense*, Phys. Scr. **95** (2020), no. 7, 075218, DOI: https://doi.org/10.1088/1402-4896/ab96e0.
[25] N. Djeddi, S. Hasan, M. Al-Smadi, and S. Momani, *Modified analytical approach for generalized quadratic and cubic logistic models with Caputo-Fabrizio fractional derivative*, Alexandr. Eng. J. **59** (2020), no. 6, 5111–5122, DOI: https://doi.org/10.1016/j.aej.2020.09.041.
[26] Q. Ding and P. J. Y. Wong, *A higher order numerical scheme for solving fractional Bagley-Torvik equation*, Math. Methods Appl. Sci. **45** (2022), 1241–1258.
[27] L. Shi, S. Tayebi, O. Abu Arqub, M. S. Osman, P. Agarwal, W. Mahamoud, et al., *The novel cubic B-spline method for fractional Painlevé and Bagley-Trovik equations in the Caputo, Caputo-Fabrizio, and conformable fractional sense*. Alexandria Eng. J. **65** (2023), 413–426.
[28] H. Fazli, H. Sun, S. Aghchi, and J. J. Nieto, *On a class of nonlinear nonlocal fractional differential equations*, Carpathian J. Math. **37** (2021), 441–448.
[29] C. L. Li and M. Cui, *The exact solution for solving a class nonlinear operator equations in the reproducing kernel space*, Appl. Math. Comput. **143** (2003), 393–399.
[30] G. N. Gumah, M. F. M. Naser, M. Al-Smadi, and S. K. Al-Omari, *Application of reproducing kernel Hilbert space method for solving second-order fuzzy Volterra integro-differential equations*, Adv. Differential Equations **2018** (2018), 475.
[31] M. Al-Smadi, H. Dutta, S. Hasan, and S. Momani, *On numerical approximation of Atangana-Baleanu-Caputo fractional integro-differential equations under uncertainty in Hilbert Space*, Math. Model. Nat. Phenom. **16** (2021), 41, DOI: https://doi.org/10.1051/mmnp/2021030.
[32] C. Li and M. Cui, *The exact solution for solving aclass nonlinear operator equations in the reproducing kernel space*, Appl. Math. Comput. **143** (2003), 393–399.
[33] M. Al-Smadi, O. Abu Arqub, N. Shawagfeh, and S. Momani, *Numerical investigations for systems of second-order periodic boundary value problems using reproducing kernel method*, Appl. Math. Comput. **291** (2016), 137–148.
[34] M. Al-Smadi, S. Momani, N. Djeddi, A. El-Ajou, and Z. Al-Zhour, *Adaptation of reproducing kernel method in solving Atangana-Baleanu fractional Bratu model*, Int. J. Dyn. Control. **11** (2023), 136–148. DOI: https://doi.org/10.1007/s40435-022-00961-1.

[35] X. Li and B. Wu, *Error estimation for the reproducing kernel method to solve linear boundary value problems*, J. Comput. Appl. Math. **243** (2013), 10–15.

[36] M. Al-Smadi, *Reliable numerical algorithm for handling fuzzy integral equations of second kind in Hilbert spaces*, Filomat **33** (2019), no. 2, 583–597, DOI: https://doi.org/10.2298/FIL1902583A.

[37] M. Al-Smadi, N, Djeddi, S. Momani, S. Al-Omari, and S. Araci, *An attractive numerical algorithm for solving nonlinear Caputo-Fabrizio fractional Abel differential equation in a Hilbert space*, Adv. Differential Equations **2021** (2021), 271, DOI: https://doi.org/10.1186/s13662-021-03428-3.

[38] S. Momani, N. Djeddi, M. Al-ŘSmadi, and S. Al-Omari, *Numerical investigation for Caputo-Fabrizio fractional Riccati and Bernoulli equations using iterative reproducing kernel method*, Appl. Numer. Math. **170** (2021), 418–434.

[39] S. Hasan, M. Al-Smadi, H. Dutta, S. Momani, and S. Hadid, *Multi-step reproducing kernel algorithm for solving Caputo-Fabrizio fractional stiff models arising in electric circuits*, Soft Computing **26** (2022), no. 2, 3713–3727, DOI: https://doi.org/10.1007/s00500-022-06885-4.

[40] M. Al-Smadi and O. Abu Arqub, *Computational algorithm for solving Fredholm time-fractional partial integro differential equations of Dirichlet functions type with error estimates*, Appl. Math. Comput. **342** (2019), 280–294.

[41] H. Xu, L. Zhang, and G. Wang, *Some new inequalities and extremal solutions of a Caputo-Fabrizio fractional Bagley-Torvik differential equation*, Fractal Fract. **6** (2022), 488.

[42] M. Al-Smadi, S. Al-Omari, Y. Karaca, and S. Momani, *Effective analytical computational technique for conformable time-fractional nonlinear Gardner equation and Cahn-Hilliard equations of fourth and sixth order emerging in dispersive media*, J. Funct. Spaces, **2022** (2022), 4422186, DOI: http://dx.doi.org/10.1155/2022/4422186.

[43] G. Gumah, K. Moaddy, M. AL-Smadi, and I. Hashim, *Solutions to uncertain Volterra integral equations by fitted reproducing kernel Hilbert space method*, J. Funct. Spaces **2016** (2016), 2920463, DOI: http://dx.doi.org/10.1155/2016/2920463.

[44] M. Al-Smadi, S. Al-Omari, S. Alhazmi, Y. Karaca, and S. Momani, *Novel travelling-wave solutions of spatial-temporal fractional model of dynamical Benjamin-Bona-Mahony system*, Fractals **31** (2023), no. 10, 2340189, DOI: https://doi.org/10.1142/S0218348X23401898.

[45] M. Alabedalhadi, S. Al-Omari, M. Al-Smadi, S. Momani, and D. L. Suthar, *New chirp soliton solutions for the space-time fractional perturbed Gerdjikov-Ivanov equation with conformable derivative*, Appl. Math. Sci. Eng. **32** (2024), 2292175, DOI: https://doi.org/10.1080/27690911.2023.2292175.